Morphology and Orientation Selection of Non-Metallic Inclusions in Electrified Molten Metal

Journal Item

Published in Metallurgical and Materials Transactions B DOI: 10.1007/s11663-017-1028-3

Morphology and Orientation Selection of Non-Metallic Inclusions in Electrified Molten Metal

Z.C. Zhao and R.S. Qin

School of Engineering & Innovation, The Open University, Walton Hall, Milton Keynes MK7 6AA, UK

Abstract

The effect of electric current on morphology and orientation selection of non-metallic inclusions in molten metal has been investigated using theoretical modelling and numerical calculation. Two geometric factors, namely the circularity (f_c) and alignment ratio (f_e) were introduced to describe the inclusions shape and configuration. Electric current free energy was calculated and the values were used to determine the thermodynamic preference between different microstructures. Electric current promotes the development of inclusion along the current direction by either expatiating directional growth or enhancing directional agglomeration. Reconfiguration of the inclusions to reduce the system electric resistance drives the phenomena. The morphology and orientation selection follows the routine to reduce electric free energy. The numerical results are in agreement with our experimental observations.

Keywords: Inclusions; Molten metal, Shape factor; Electric current

*Corresponding author e-mail: rongshan.qin@open.ac.uk

I. INTRODUCTION

Inclusion management has been a challenging topic in alloys processing for many decades.[1,2] Cleanliness concerns the volume fraction and size-distribution of non-metallic inclusions resident in the engineering components.[3-4] Smaller volume fraction and smaller dimension of inclusion are desirable in clean metal fabrication. The morphology, orientation and configuration of inclusions also affect the microstructure refinement in subsequent thermomechanical processing and mechanical performance in engineering service.[5] Inclusions provide heterogeneous nucleation sites in solidification and recrystallization.[6-7] The morphology (e.g. the curvature of the tip) of inclusions affects the heterogeneous critical nucleation size. The orientation of the inclusions affects the stress and strain distributions under directional loading.[5,8]

The morphology and orientation of inclusions are determined by the growth of individual inclusions and coalescence between inclusions. Most inclusions are non-metallic oxides which have been formed during extraction, liquid metal processing and liquid-solid phase transition in the open environments.[9-10] Some of the inclusions are formed even in a protected environment due to the contaminant of non-metallic components such as O, N and S elements in the liquid metal.[11] The growth and coalescence are determined by the system thermodynamics and kinetics.[9] A significant amount of works have been devoted to understand the phenomena in the environmental constrains without electric field. This includes how the growth and coalescences are affected by the temperature, chemical constitution, convection, and other factors.[12] When the materials are subjected to electric field, the thermodynamics and kinetics to the inclusion growth and coalescence between inclusions are associated to the implemented electric field.[13-14] It has been revealed that the non-metallic spherical

inclusions are driven toward the walls of liquid metal by the passing electric current,[15-18] toward separation in a direction perpendicular to the current direction, and toward agglomeration when the distance between inclusions is within a critical value and inclusions are aligned along the current flow.[19] The arrangement of inclusion in electrified metals can prevent the clogging of nozzles.[20-23]

The present work aims to study the effect of electric current on the morphology and morphological orientation selection of non-metallic inclusions in liquid metal. As a primary study, the thermodynamic stability of inclusions with various geometry and configuration has been investigated in the present work. The morphological evolution of an inclusion can be derived from its thermodynamic stability. The kinetics for interface evolution during crystal growth under electric field has been studied by Klinger and Levin.[24] The modelling of inclusions microstructure and computation of electric current effect in the system is presented in section II. The numerical calculation and results are presented in section III. Section IV summarises the research with some conclusions and remarks.

II. MODELLING AND COMPUTATIONAL METHOD

For a system carrying electric current, there are two eigendirections, namely the parallel and perpendicular directions to that of the electric current. For this consideration, we consider a cylindrical shape inclusion with its axis of symmetry along z-axis in a Cartesian coordinates. The electric field is along x axis and the transverse direction along y axis. One introduces circularity (f_c) to represent the geometry of cylindrical inclusion by

$$f_c = \frac{4\pi A}{P^2} \qquad [1]$$

where A is the cross section area and P the cross section pattern perimeter. Circular cross area has larger circularity than that of elliptic one. The fractal surface,[25] e.g. dendrite, has a value of f_c approaching to zero. The alignment ratio (f_e) is defined as

$$f_e = \sqrt{\frac{I_x}{I_y}} \qquad [2]$$

where I_x and I_y are moment of inertia to principal axis x and y respectively. The moment of inertia to a principal axis *I* is an indicator of mass distribution and is defined as

$$I = \int d^2 \delta m \qquad [3]$$

where m is mass and d is the distance toward the principal axis. In a discrete space I is obtainable by

$$I = \sum m_i d_i^2 \qquad [4]$$

where i indicate the *i-th* cell. The closer the mass is distributed toward the axis, the smaller the moment of inertia is.

Non-metallic inclusions have higher electrical resistivity than that of the liquid metal matrix. Electric currents change their flow direction when passing through the inclusions. Different inclusion morphologies and orientations lead to different electric current density distribution in the system. The current density $\vec{j}(r)$ is determined by the local electrical conductivity $\sigma(r)$ and electrical potential gradient $\nabla\phi(r)$ via Ohm's law

$$\vec{j}(r) = -\sigma(r)\nabla\phi(r) \qquad [5]$$

where r is a point in three-dimensional space. The electric current free energy has been derived from a starting point of the work done by the applied electric field to the drift of electrons of the given microstructure under static conditions. The detailed derivation

procedures have been presented by Qin and Bhowmik.[26], but the application of the similar format in discussion of electric-current-induced phase transformation can be traced back to decades ago.[27,28] The general format of electric current free energy corresponding to each configuration is shown in the following equation:[26]

$$G_e = -\frac{1}{8\pi}\int_V \int_V \frac{\mu(r')\vec{j}(r')\cdot\vec{j}(r)}{|r-r'|}drdr' \quad [6]$$

where μ is the magnetic permeability of the phase. r and r' represent different points in materials. The integration of each point goes throughout the whole system.

Numerical computations are conducted using an in-house developed C++ code package to obtain current density distribution $\vec{j}(r)$ and electric current free energy G_e. The code is based on a numerical relaxation method and using time iteration to find the numerical solution for electric current density distribution and using direct summation to find the integration value of electric current free energy.[26] The space is discretized into cubic cells and each cell is occupied by either inclusion or liquid metal. The zero thickness interface assumption is made and electricity conductivity between cell α and β is

$$\sigma_{\alpha\beta} = \frac{2\sigma_\alpha\sigma_\beta}{\sigma_\alpha + \sigma_\beta} \quad [7]$$

The electrical potential of inclusions (ϕ_i) and liquid metal (ϕ_m) obeys Laplace equations

$$\Delta\phi_i(r) = 0 \quad [8.1]$$

$$\Delta\phi_m(r) = 0 \quad [8.2]$$

At the inclusion-liquid metal interface, ϕ_i and ϕ_m satisfy the following boundary conditions

$$\phi_i = \phi_m \quad [8.3]$$

$$\sigma_i \nabla_n \phi_i = \sigma_m \nabla_n \phi_m \quad [8.4]$$

The electrical potential distribution is calculated via relaxation method of iterating the following equation

$$\phi_\alpha = \frac{\sum \phi_\beta \sigma_{\alpha\beta}}{\sum \sigma_{\alpha\beta}} \quad [9]$$

Substituting the numerical results of electrical potential distribution into Eq. [5], the electric current distribution is obtained. Numerically integrating the electric current distribution in space according to Eq. [6] will obtain the electric current free energy. The discrete format of Eq. [6] is as following [26, 29]

$$\Delta G_e = -\frac{1}{8\pi} \sum_\alpha \sum_\gamma \frac{\mu(r_\alpha)\vec{j}(r_\alpha) \cdot \vec{j}(r_\gamma) V_\alpha V_\gamma}{|r_\alpha - r_\gamma|} \quad [10]$$

where V_α and V_γ are the volume of lattice-α and lattice-γ, respectively.

An inclusion taking different morphologies corresponds to different thermodynamic stability. The system free energy differences include the interfacial free energy difference and electric current free energy differences. The chemical free energy is related to the volume fraction of inclusion and hence is the same for different inclusion morphologies. The interfacial free energy is the product of interface tension and interface area. The former is the same if interface anisotropy is negligible. The interface area is different for different morphologies. The interfacial free energy difference can be calculated straightforwardly. The electric current free energy differences for different inclusion morphologies can be calculated numerically using equation [10].

III. NUMERICAL CALCULATION AND RESULTS

Polygon cylinder with equal height and cross section area but with different cross section shape is used to simulate different inclusion particle configuration. The setup of the system is illustrated schematically in Fig.1. The inclusion particle is positioned in the centre of liquid metal matrix and the electric voltage is applied horizontally. The electrical conductivity of liquid metal matrix and inclusion are chosen to be 10^5 $\Omega^{-1}m^{-1}$ and 10^2 $\Omega^{-1}m^{-1}$ after reference that of liquid steel and MnS,[15, 17-18] respectively. The computational logistic domain contains 300×120×11 lattices with lattice distance 10^{-3}m. Each cylindrical inclusion is 3×10^{-3}m in height and $25\times10^{-3}m^2$ in cross area. 20V electrical potential differences are implemented to the computational domain along x (longest) axis.

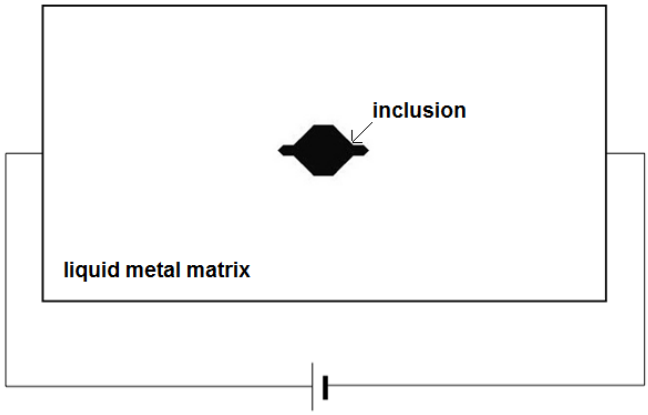

Fig. 1—A schematic diagram for the configuration of inclusions in electrified matrix

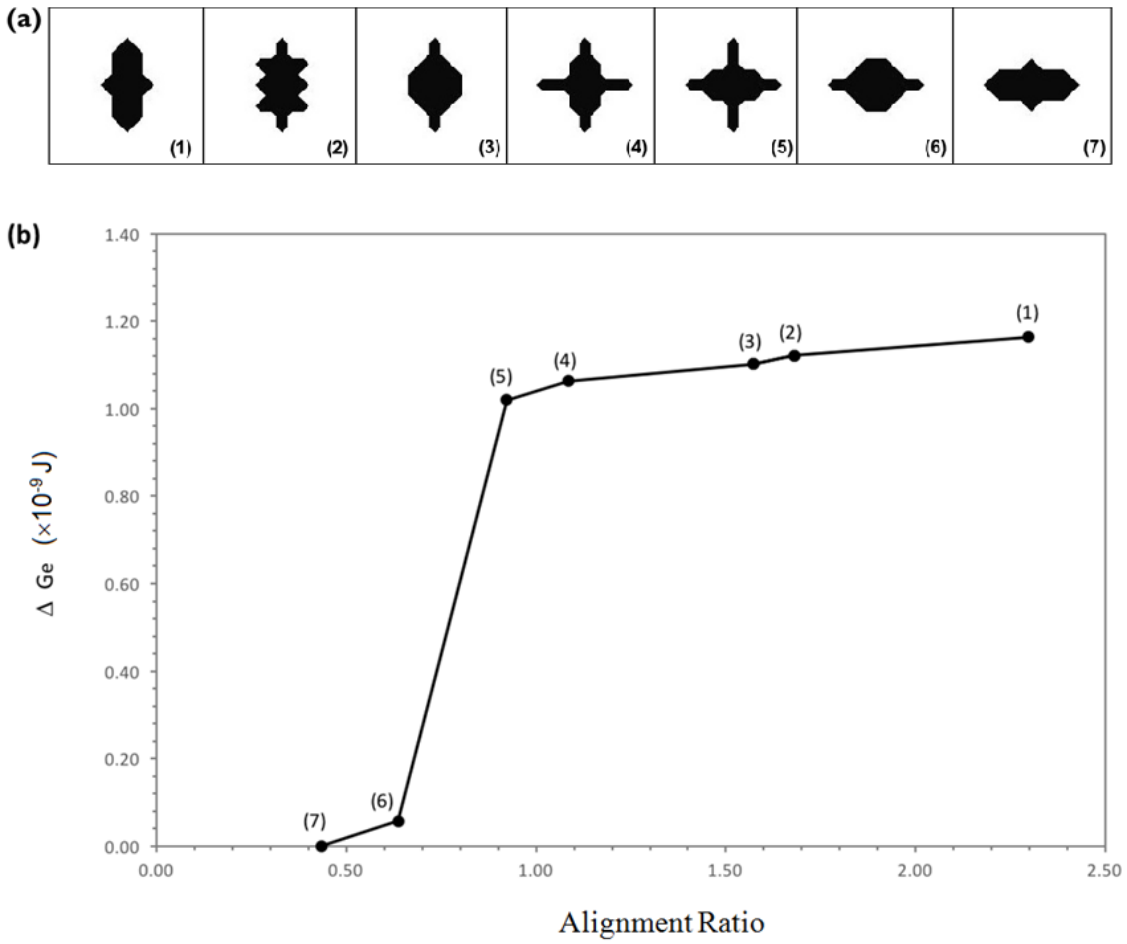

Fig. 2—The relative electric current free energy for various inclusion morphologies and orientations: (a) the geometries and orientations of an inclusion; (b) The change of electric current free energy with respect to the alignment ratio.

Fig. 2(a) demonstrates the inclusions with different morphologies at their cross section. Their alignment ratios in Fig. 2(a) decrease monotonically from shape (1) to shape (7). One chooses the electric free energy of shape (7) as the reference state. The relative electric current free energies for all 7 cases listed in Fig. 2(a) are calculated and plotted in Fig. 2(b). The alignment ratio represents the orientation of an inclusion along the electric current direction. Fig. 2(b) shows that a shape with smaller alignment ratio has smaller electric current free energy. In another word, electric current promotes an orientation of the inclusion along the current direction and retard the inclusion to the

orientation perpendicular to the current direction.

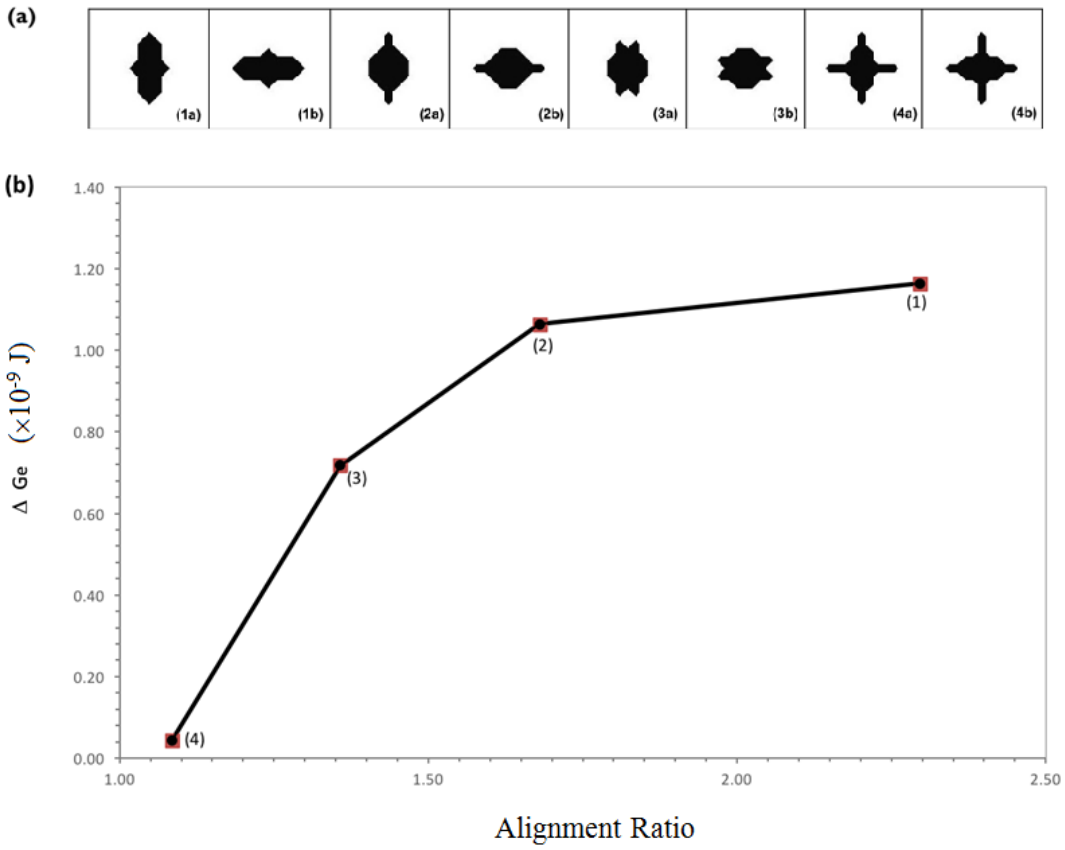

Fig. 3—The change of inclusions shapes and corresponding electric current free energy change. (a) 4 types of inclusions with their longest principal axis perpendicular or parallel to the electric current, respectively. (b) The change of electric current free energy only when the inclusions are rotated 90°.

It can be seen from Fig.2 that the electric current free energy increases as the alignment ratio to increase. The increase of alignment ratio is contributed by both the increase in moment of inertia to principal axis x (parallel to electric current) and decrease in moment of inertia to principal axis y (perpendicular to the electric current). In addition, a significant free energy drop is observed from inclusion configuration 5 to 6, which corresponds to the longest principal axis change from the direction perpendicular to

electric current to parallel to that. The interface area of polygon cylinder is the sum of two cross section areas and one lateral area which is the product of height and perimeter of cross section. The simulated shapes are polygon cylinder with equivalent cross section and height. In the simulation case, if the perimeter of cross section keeps the same, the inclusions have same interface area and hence the same interfacial free energy. In the above group, the perimeters of configurations 2, 4 and 5 are the same with a value of 0.24 while the perimeters of configurations 1, 3, 6, and 7 are the same with a value of 0.4. It is clear that, even on the condition of same interface free energy, the same trend of electric current free energy change is followed.

Fig. 3(a) shows 4 types of inclusion's morphologies with their longest principal axes either perpendicular (ia, i=1,2,3,4) or parallel (ib) to the electric current direction. One has chosen the orientation ib as the thermodynamic reference state and calculated the relative electric current free energy of (ia). In Fig. 3(b), the horizontal axis is the alignment ratio of ib and the vertical axis is the relative electric current free energy of ia regarding to ib. Fig. 3(b) shows that, the bigger the alignment ratio the larger the difference of free energy between its different orientations. The all-positive values of free energy change also indicate that the inclusions prefer to be positioned with the longest principal axis along the electric current.

Fig. 4(a) shows a group of inclusion's morphologies to evolve toward the reduction of their moment of inertia to principal axis x. The alignment ratios are all large than 1 and the thermodynamic reference state is set as that of in Fig. 4(a5). Fig. 4(b) shows the decrease of relative free energy with the decreased alignment ratio. This calculation shows that electric current retards the development of inclusion's morphology in the

direction perpendicular to the current direction.

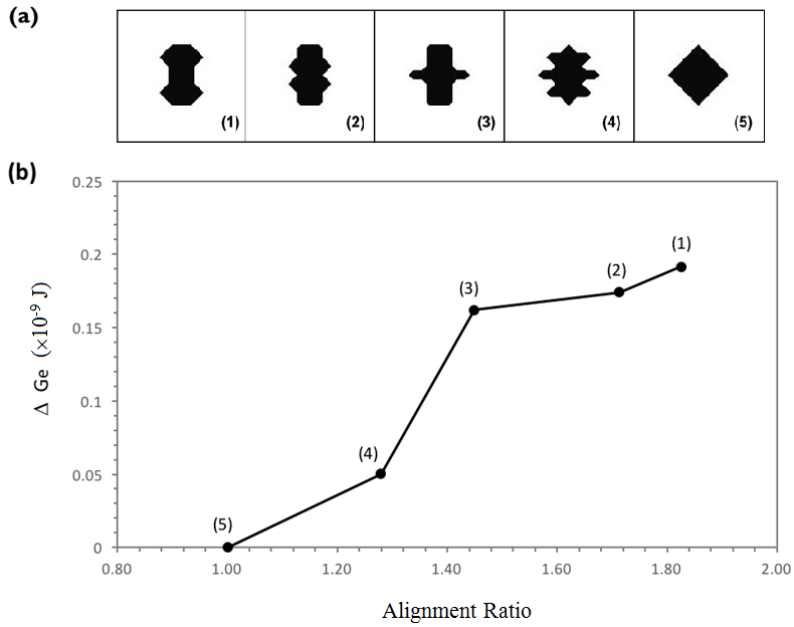

Fig. 4—The change of inclusions moments and corresponding electric current free energy change. (a) A set of inclusions with moment of inertia to principal axis x to change; (b) The change of electric current free energy with respect to alignment ratio.

Fig 5(a) presents the change of inclusion's morphology to reduce the moment of inertia to principal axis y from shape (1) to shape (3). The agglomeration of two inclusions along electric current direction is similar to this case. In this group of inclusions, the alignment ratios are smaller than 1 and no change of moment of inertia to principal axis x. It can be seen from Fig. 5(b) that the electric current free energy decreases as the alignment ratio increases. It is worth to mention that no interfacial energy change is involved in this set of simulation. The perimeter for those morphologies is 28mm. This corresponds to circularity 0.4.

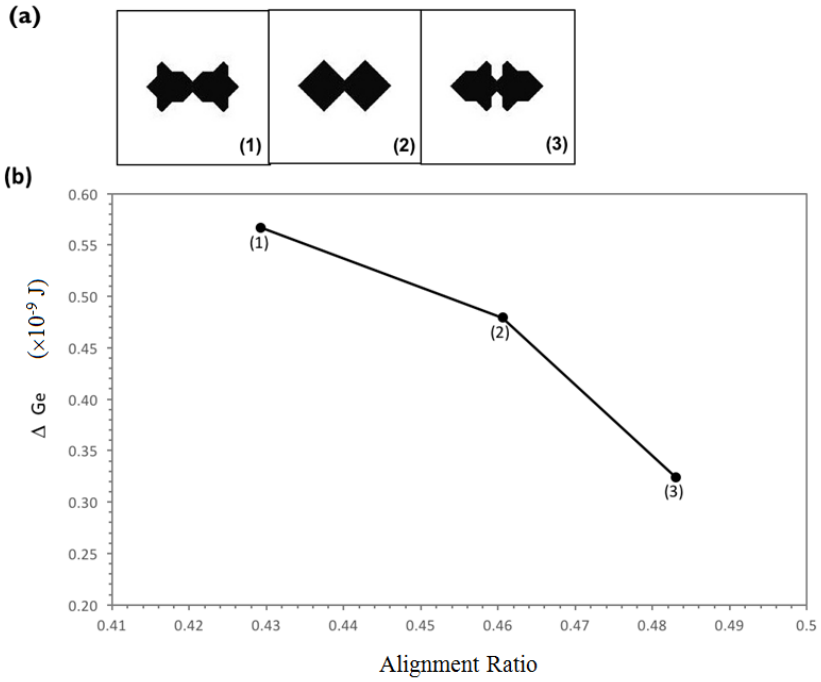

Fig. 5—The change of inclusions morphology and corresponding electric current free energy change. (a) A set of inclusion's morphology with moment of inertia to principal axis y to reduce; (b) The change of electric current free energy with respect to alignment ratio.

The combination of above simulation results show that the thermodynamic preferred state of inclusions morphology and orientation is inclusion elongated along electric current, which is in agreement with experiment result.[30] After electric current treatment, the morphology of inclusions are long rods or ellipsoid with longest axis along the direction parallel to the electric current.

IV. CONCLUSIONS

The effect of electric current on the morphology and orientation selections of non-metallic inclusions has been studied. The numerical calculations reveal that the inclusion morphologies with different circularities and different orientations regarding

to the electric current direction possess different thermodynamic stabilities under electric current. Alignment ratio, which measures the ratio between moments of inertia to axes parallel and perpendicular to the current direction, is able to indicate the preferred configuration of non-metallic inclusions in liquid metal. This can be summarized as follows

- An inclusion with higher alignment ratio is with higher electric current free energy. The morphological selection of inclusion under electric current is toward the lower alignment ratio.
- An inclusion with same morphology tends to orient toward the electric current direction. Electric current promotes the rotation of an inclusion toward the reduction of its alignment ratio.
- Electric current promotes the inclusions to reduce its moments of inertia to electric current axis when the liner dimension along the axis perpendicular to the current direction is unchanged. Electric current also promotes the inclusions to reduce its moments of inertia to axis perpendicular to electric current direction.

Acknowledgements

The work was financially supported by EPSRC (EP/L00030X/1) and the Royal Society Newton Advanced Fellowship (NA150320).

References

1. L.F. Zhang and B.G. Thomas: *ISIJ Int*., 2003, vol. 43, pp. 271-291.
2. H.V. Atkinson and G. Shi: *Prog. Mater. Sci*. 2003, vol. 48, pp. 457-520.

3. L.F. Zhang, J. Aoki and B.G. Thomas: *Metall. Mater. Trans. B*, 2006, vol. 37B, pp. 361-379.
4. G. Shi, H.V. Atkinson, C.M. Sellars, C.W. Anderson and J.R. Yates: *Acta Mater*. 2001, vol. 49, pp. 1813-1820.
5. L. Liu and F.H. Samuel: *J Mater. Sci.*, 1998, vol. 33, pp. 2269-2281.
6. J. M. Gregg and H. K. D. H. Bhadeshia: *Acta Mater.*, 1997, vol. 45, 739–748.
7. K.M. Wu, Y. Inagawa and M. Enomoto: *Mater. Charact.* 2004, vol.52, pp. 121-127.
8. J. Eshelby: *Proc. R. Soc. London Sect. A* 1957, vol. 241A, pp. 376-396.
9. Z.Y. Deng, M.Y. Zhu and S.C. Du: *Metall. Mater. Trans. B*, 2016, vol. 47B, pp. 3158-3167
10. C. Gatellier, H. Gaye, J. Lehmann, J.N. Pontoire and P. V. Riboud: *Steel Res*. 1993, vol. 64, pp. 87-92.
11. S.A. Decterov, Y.B. Kang and I.H. Jung: *J Phase Equilib Diff*. 2009, vol.30, pp. 443-461.
12. M. Suzuki, R. Yamaguchi, K. Murakami and M. Nakada: *ISIJ Inter*. 2001, vol. 41, pp. 247-256.
13. R. S. Qin: *Mater. Sci. Technol.* 2015, vol. 31, pp. 203-206.
14. R. S. Qin, A. Rahnama, W. J. Lu, X. F. Zhang and B. Elliott-Bowman: *Mater. Sci. Technol*., 2014, vol. 30, pp. 1040–1044.
15. X.F. Zhang, W.J. Lu and R.S. Qin: *Scr. Mater*., 2013, vol. 69, pp.453-456.
16. S. Taniguchi and J.K. Brimacombe: *ISIJ Inter*., 1994, vol. 34, pp. 722-731.
17. X. F. Zhang and R. S. Qin: *Sci Rep*., 2015, vol.5, pp.10162
18. X. F. Zhang and R. S. Qin: *Appl. Phys. Lett*., 2014, vol. 104, pp. 114106.

19. Z.C. Zhao and R.S. Qin: *Mater. Sci. Technol*., 2017, doi 10.1080/02670836.2016.1270729.
20. M. Li and R. I. L. Guthrie: *Metall. Mater. Trans*. B, 2000, vol. 31B, pp. 855-866.
21. W. B. Dai, J. K. Yu, C. M. Du, L. Zhang and X. L. Wang: *Mater. Sci. Technol*., 2015, vol. 31, pp. 1555–1559.
22. R. I. L. Guthrie: *Mater. Trans. B*. 2001, vol. 32B, pp. 1067-1079.
23. W. B. Dai, X. L. Zhou, X. Yang, G. P. Tang, D. B. Jia, N. L. Cheng and J. K. Yu: *Acta Metall. Sinica-English Lett*., 2016, vol. 29, pp. 500–504.
24. L. Klinger and L. Levin: *J. App. Phys*., 1995, vol. 78, pp. 1669–1672.
25. R.S. Qin and Z. Fan: *Mater. Sci. Technol*., 2001, vol. 17, pp. 1149-1152.
26. R.S. Qin, A. Bhowmik: *Mater. Sci. Technol.*, 2015, vol.31, pp.1560-1563.
27. Y. Dolinsky, T. Elperin: *Phys. Rev. B*, 1994, vol.50, pp.52–58.
28. R.S. Qin, B.L. Zhou: *Int. J. Non-Equilib. Proc*., 1998, vol.11, pp.77-86.
29. R.S. Qin: *Sci. Rep.*, 2017, vol. **7**, pp. 41451.
30. X.F. Zhang, W.J. Lu and R.S. Qin: *Phil. Mag. Lett*., 2015, vol. 95, pp. 101-109.

List of figure captions

Fig. 1—A schematic diagram for the configuration of inclusions in electrified matrix

Fig. 2—The relative electric current free energy for various inclusion morphologies and orientations: (a) the geometries and orientations of an inclusion; (b) The change of electric current free energy with respect to the alignment ratio.

Fig. 3—The change of inclusions shapes and corresponding electric current free energy change. (a) 4 types of inclusions with their longest principal axis perpendicular or parallel to the electric current, respectively. (b) The change of electric current free energy only when the inclusions are rotated 90°.

Fig. 4—The change of inclusions moments and corresponding electric current free energy change. (a) A set of inclusions with moment of inertia to principal axis x to change; (b) The change of electric current free energy with respect to alignment ratio.

Fig. 5—The change of inclusions morphology and corresponding electric current free energy change. (a) A set of inclusion's morphology with moment of inertia to principal axis y to reduce; (b) The change of electric current free energy with respect to alignment ratio.